

Supplementary Materials for

Integration of Activating and Inhibitory Receptor Signaling by Regulated Phosphorylation of Vav1 in Immune Cells

Sven Mesecke, Doris Urlaub, Hauke Busch, Roland Eils,* Carsten Watzl*

*To whom correspondence should be addressed. E-mail: r.eils@dkfz.de (R.E.); watzl@uni-hd.de (C.W.)

Published 31 May 2011, *Sci. Signal.* **4**, ra36 (2011)

DOI: 10.1126/scisignal.2001325

This PDF file includes:

Methods

Fig. S1. Quantification of cytosolic proteins by Western blotting analysis.

Fig. S2. Initial simulation results.

Fig. S3. Interclass parameter ratios.

Fig. S4. Results of the parameter fit for all 72 models.

Fig. S5. Quantification of the total amounts of pVav1 and pSFK after stimulation of NK cells.

Fig. S6. Comparison between predicted and experimentally observed pVav1 responses after treatment with PP1.

Table S1. Kinetic parameters used for modeling.

Table S2. Protein numbers and concentrations for different NK cell types.

Table S3. Table of shape functions and their analytical equations used for the classification of shapes generated in the parameter scan.

Table S4. Literature-derived and fitted kinetic rates.

References

Other Supplementary Material for this manuscript includes the following:

(available at www.sciencesignaling.org/cgi/content/full/4/175/ra36/DC1)

MATLAB and SBML model files (.m and .xml format).

Methods

Quantification of protein concentrations

Surface molecules were quantified with Qifikit (Dako), according to the manufacturer's protocol. Cytoplasmic proteins were quantified by quantitative Western blotting analysis with the recombinant proteins GST-tagged, full-length Lck (Abnova) and full-length SHP-1 (Millipore) as standards. To produce a His-tagged N-terminal portion of Vav1 (amino acid residues 2 to 462), we used PCR to amplify the corresponding sequence from complementary DNA (cDNA) from primary human NK cells and sub-cloned it into the pRSet B Vector (Invitrogen). The protein was over-expressed in *Escherichia coli* BL21-DE3 PLysS cells (Invitrogen) and purified under denaturing conditions. Protein concentration was determined with the EZQ Protein Quantitation Kit (Molecular Probes), according to the manufacturer's instructions, and purity was assessed by SDS-PAGE and Silver Staining (Silver SNAP Stain Kit, Thermo). For semi-quantitative analysis of tyrosine phosphorylation, cells were stimulated for 10 min at 37°C with pervanadate [0.2 mM activated orthovanadate (Sigma), 0.3% H₂O₂ in phosphate-buffered saline (PBS)] for maximum phosphorylation, or were preincubated for 30 min at 37°C with PP1 (20 μM, Biomol) for minimal phosphorylation. Cells were then lysed. By diluting the lysate of pervanadate-stimulated cells with the lysates from PP1-treated cells, we generated a standard curve, and used quantitative Western blotting analysis of the lysates of NKG2D- or NKG2A-stimulated NK cells to make comparisons.

Description of the mathematical model

Theoretical arguments and experimental evidence dictate that possible biochemical reactions occur at all times. Even in chemical equilibrium, there are forward and reverse reactions between proteins. These reactions establish the unstimulated, yet responsive and basally active cellular ground state, as can be seen by the presence of phosphorylated forms of Vav1, Lck, and SHP-1 under unstimulated conditions. The activity of SFK members is inhibited by intramolecular binding of the SH2 domain to an autoinhibitory phosphotyrosine. To become activated, SFKs must release this conformation, which can occur by intermolecular binding to phosphorylated tyrosine residues (pTyr), for example, on receptors; however, in their autoinhibited state, SFKs cannot bind to pTyr residues on other molecules. Therefore, an SFK must be released from its autoinhibited conformation from time to time to be able to bind to other pTyr residues. This release establishes a pool of active, non-autoinhibited SFKs, which phosphorylate their substrates at a basal rate, establishing some steady-state level of phosphorylation. An external stimulus perturbs this ground state, and the system can move to a new stimulated state. A model describing this system therefore has to account for the unstimulated (homeostatic) and the stimulated states, and requires a mechanism for the external perturbation of the ground state.

Spatial aspects of NK cell signaling

NK cell signaling occurs in vivo upon direct cell-cell contact; however, signaling can also be triggered in vitro by antibody-covered beads or by antibody-mediated cross-linking of receptors. Common to all these stimuli is the reduction of the mean distance between adjacent receptors. Upon making contact with the target cell, a highly complex and dynamic supramolecular assembly called the immunological synapse (IS) is established at the contact site between the NK cell and the target cell. Our method of antibody-mediated cross-linking of receptors similarly induces receptor clusters, which are concentrated at one location within the plasma membrane. To incorporate this anisotropy into our model, we represented space with three discrete, well-mixed compartments: (i) the "cytoplasm," that is, a volume given by the measured diameters of NK cells from which is subtracted the volume of the NK cell nucleus and the volume of a hypothetical shell around the cell membrane; (ii) the "membrane," that is, a volume given by assuming a shell with a diameter approximately the

size of the extension of transmembrane proteins into the cytoplasm; and (iii) the IS, that is, a volume given by the size of ISs in NK–target cell conjugates and the diameter of the hypothetical shell in (ii). The resulting volumes for different cell types were determined (fig. S1). All of the reactions occur between states that reside in the same compartment. Molecule exchanges between compartments were modeled as first-order reactions between corresponding molecules, that is, the molecule in the IS compartment (for example, Vav_is) reacts in a first-order reaction to the corresponding molecule in the membrane compartment (Vav_m). We did not assume different diffusion rates for the different molecules modeled in our approach so as to limit potential sources of nonlinearity to the network topology alone. All measured protein concentrations were at the same level as or below the Michaelis-Menten constant (K_M) for the corresponding reactions, which enabled us to reduce the enzyme reactions to pseudo-bimolecular reactions with the kinetic constant k_{cat}/K_M . As there is little evidence that conformational changes are causative for cytoplasmic signaling, we consider inter-receptor distance reduction as necessary and sufficient. This is included in our model by limiting ligand-receptor association to the immunological synapse, which leads to an increase in the local receptor concentration by passive diffusive entrapment.

Molecules and reactions included in the model

Our model incorporates only a small receptor-proximal part of the NK cell signaling pathway. The model includes the activating receptor NKG2D with its signaling adaptor protein DAP10, modeled as four pseudo molecules with one phosphorylation site each (to avoid the combinatorial complexity that arises from one NKG2D dimer coupled to a DAP10 tetramer with four phosphorylation sites altogether), and the inhibitory receptor complex CD94-NKG2A, which has one phosphorylation site. The transmembrane receptors are localized in the membrane and IS compartments. They can associate and dissociate with their respective ligands by a bimolecular reaction in the IS.

The receptors are phosphorylated by SFKs regardless of their location or binding state. As stated earlier, it is likely that SFKs constantly switch between a closed (auto-inhibited) and an open (active) form to maintain a state in which they can react to external perturbations. Therefore, we include a rapidly equilibrating intermolecular conformational change from an open to a closed conformation, and vice versa. Only the open SFK (SFKo) pool is enzymatically active. The phosphorylation event is implemented as a pseudo bimolecular reaction between SFKo and the receptors. Nonlinearities in the response of the system are thereby caused by the network topology rather than by overly complex reaction schemes (1). SFKs are membrane-bound and are confined in our model to the membrane and to the IS. The SH2 adaptor protein Grb2 can associate with DAP10 through pTyr residues and thereby recruit the guanine nucleotide exchange factor (GEF) Vav1 to pDAP10. However, for the sake of simplicity, we reduced the two-step binding process to a one-step process by including an effective Grb2:Vav1 hybrid in our model. Vav1 is phosphorylated by SFKo. This reaction is also implemented as a pseudo bimolecular reaction. SFK-dependent phosphorylation of CD94-NKG2A creates a binding pocket for SHP-1, which contains an auto-inhibitory loop similar to that of SFKs. An intramolecular binding event auto-inhibits the catalytic activity of SHP-1. This auto-inhibition can be relieved by the binding of SHP-1 to a protein that contains a tyrosine-phosphorylated ITIM. The requirement for this association to release inhibition mandates a dynamic change from an open to a closed conformation and vice versa. SHP-1 dephosphorylates pVav1 in its open conformation in our model, thereby closing the loop between the activating and inhibiting pathways.

Modules investigated

As mentioned earlier, little is known about the mechanistic details of the previously described

biochemical reactions; however, some potential mechanisms have been suggested in the literature. To investigate this ambiguity and the importance and function of the potential interactions, we constructed a combinatorial set of models from elementary modules representing these alternative hypotheses.

Actin reorganization [module (a)] refers to a potential positive feedback loop from pVav1-dependent reorganization of the actin cytoskeleton, leading to increased aggregation of activating receptors at the IS, which in turn results in enhanced recruitment of Vav1 to the IS. Because few mechanistic details are known, we assumed a fictitious reaction from pVav-1 leading to an increase in the amount of activating receptors at the IS. This was modeled as a pseudo-enzymatic reaction with pVav-1 acting as an enzyme that increases the amount of DAP10 at the IS.

Kinase-phosphatase segregation [module (b)] has been proposed and investigated as a potential non-conformational change mechanism for the outbreak from basal phosphorylation of the TCR. Taking into account the large extracellular domains of the transmembrane phosphatase CD45, it is thought that ligand-receptor interactions occur only in regions of the membrane that lack this phosphatase, thereby shifting the balance between phosphorylation and dephosphorylation towards the former. This potential mechanism could also occur in NK cells. We modeled this potential mechanism by including a pseudo-enzymatic reaction between the ligand-receptor complex and CD45 in the IS compartment, which leads to its transport to the membrane compartment.

Kinase association [modules (c) and (g)] describes the potential association of SFKs with activating (c) or inhibiting (g) phosphorylated receptors. This potential mechanism was modeled as a simple binding reaction of SFKs in their open conformation to the respective receptors.

Kinase autophosphorylation [module (d)] represents the intermolecular auto-phosphorylation of SFKs. Phosphorylated SFKs have a higher catalytic activity than do non-phosphorylated SFKs; however, the latter still have some catalytic activity, including towards other SFKs. In our model, we therefore assumed pseudo-bimolecular enzymatic reactions between all respective SFK states. This auto-phosphorylation would lead to a fully phosphorylated SFK pool without dephosphorylation events. The dephosphorylation occurs by phosphatases, such as CD45. The combination of both reactions establishes a basal level of SFK phosphorylation.

SHP-1-mediated dephosphorylation of pSFKs [module (e)] was proposed to provide an additional negative feedback to the auto-phosphorylation of SFKs introduced in module (d). It was modeled as a pseudo bimolecular enzymatic reaction between active SHP-1 and phosphorylated SFKs.

SHP-1-mediated phosphorylation [module (f)] refers to the increased SHP-1 activity upon SFK-dependent phosphorylation, and was modeled as a pseudo bimolecular reaction between active SFKs and SHP-1.

These reactions alone would lead to a fully phosphorylated cellular state. Obviously, all phosphorylated states have to be dephosphorylated. One phosphatase implicated in this reaction is CD45, which is included in the model and is assumed to dephosphorylate all phosphorylated states if accessible, that is, when unbound by another protein. Because CD45 is only localized in the IS and the membrane compartment, we also assumed the presence of a generic cytoplasmic phosphatase to dephosphorylate cytoplasmic proteins.

Determination of interclass parameter ratios

The random parameter scan (Fig. 4A) generated nine qualitatively different shapes or classes. The histogram plot of the shape distribution of the different models indicated some unique dominating shapes for each model, for example shape 6 (yellow) and shape 7 (orange) for models containing the modules c and g (SHK association with inhibiting and activating receptors). To identify crucial parameters that differ between the alternative shapes, we calculated the pair-wise ratio of parameters for each sample in the parameter set. The 5,000 parameter sets were sorted according to the shape that they produced, and for each set we divided each parameter by each other parameter. Next, we computed the geometric mean parameter ratios over all sets that generated the shape of interest. The fold ratio of these ratios between alternative shapes is plotted in a heat-map (fig. S3). An example for model c: on geometric average, the parameter $k_{a_pcd94_ashp_pcd94ashp}$ (which describes the association of SHP-1 and phosphorylated NKG2A-CD94) is 5.2×10^3 times larger than the parameter $k_{2_cd45_pvav_vav}$ (which describes the constitutive dephosphorylation of phosphorylated Vav by CD45) in shape class 6, and 6.8×10^4 times larger in shape class 9. The ratio between these parameter ratios is ~ 0.075 , or a fold ratio of around -14.

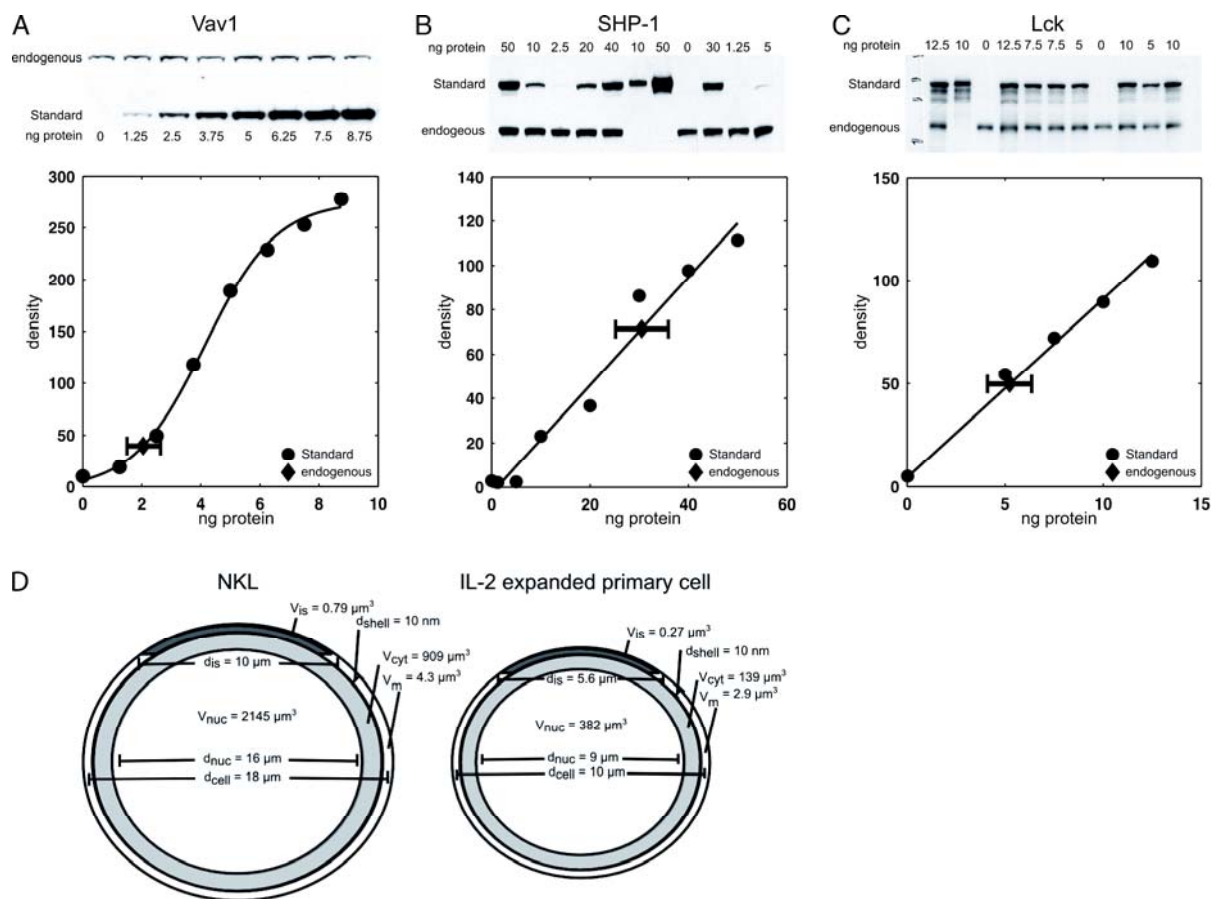


Fig. S1. Quantification of cytosolic proteins by Western blotting analysis. The amount of (A) Vav1, (B) SHP-1, and (C) Lck were measured by quantitative Western blotting with recombinant proteins as standards. Because the recombinant proteins differed in size from those of the endogenous proteins, the indicated amount of standard was diluted in cell lysates and samples were analyzed by SDS-PAGE and Western blotting. Blots were analyzed by densitometry, and a standard curve was created for the recombinant protein and compared to the signal of the endogenous protein (indicated in the standard curve by diamonds and error bars). The amount of endogenous protein per cell was calculated with the following formula: (measured mass of endogenous protein / molecular weight of recombinant protein) \times (particles per mol / amount of cells in lysate). Representative experiments are shown. Results of all quantifications are summarized in table S2. The cellular spatial dimensions (D) were used to calculate the concentrations from these quantifications. The spatial dimensions of the NK cell line NKL (left) and IL-2-expanded primary human NK cells (right) are indicated. Cell diameters were determined with a Casy cell counter (Innovatis). The volumes of each compartment were calculated from literature parameters based on the measured dimensions of the cells. V_{is} , volume of the IS; d_{shell} , approximate extension of receptors into the cytoplasm; V_{cyt} , volume of the cytoplasm; V_m , volume of the membrane compartment; d_{is} , diameter of the IS; V_{nuc} , volume nucleus; d_{nuc} , diameter nucleus; d_{cell} , diameter cell.

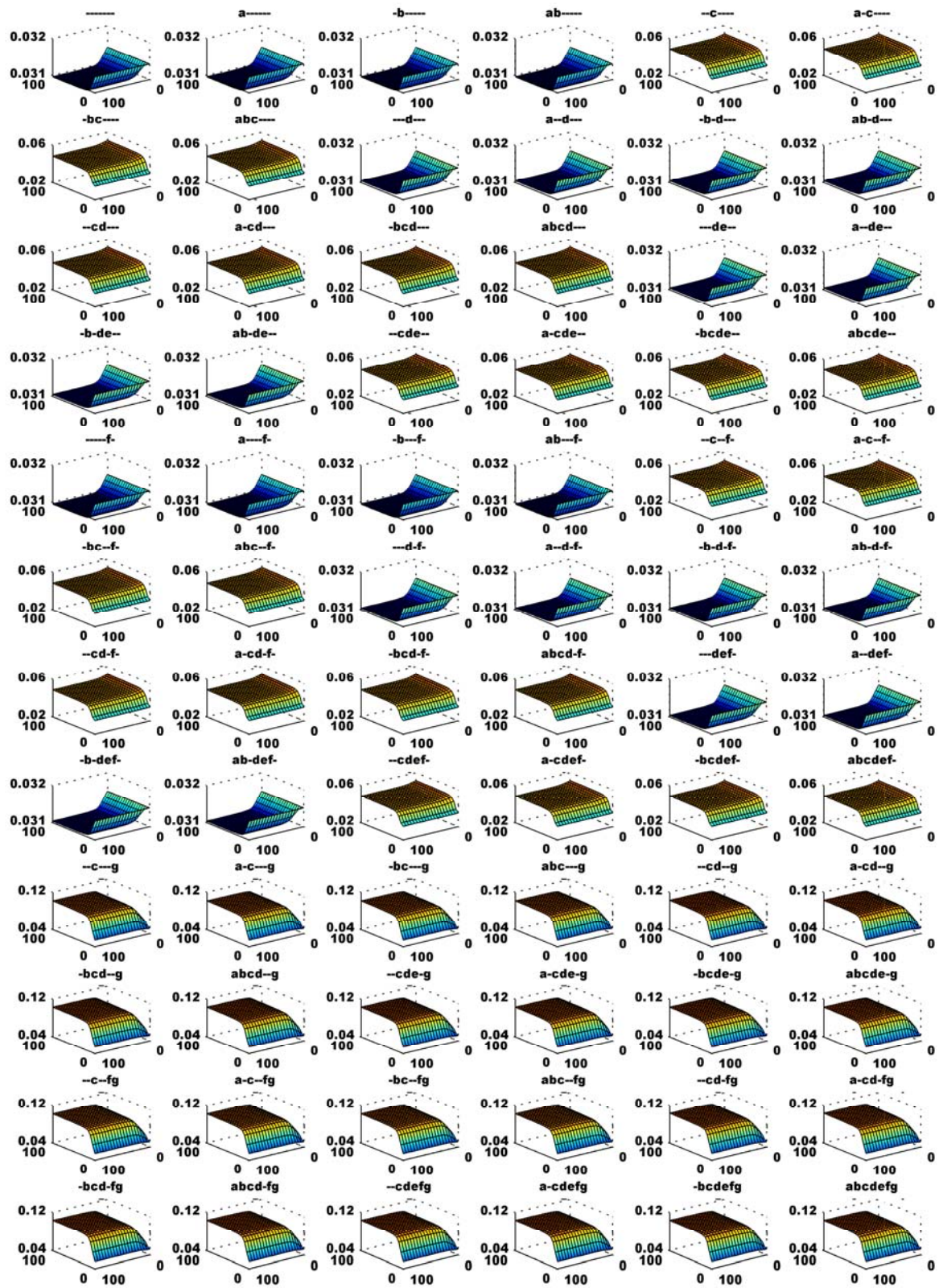


Fig. S2. Initial simulation results. The steady-state amount of pVav1 (z-axis, in nM) was determined for all 72 different models (module code indicated on the top according to Fig. 1) with the geometric mean of the values for kinetic parameters shown in table S1 (see the first column in table S4) for varying amounts of inhibitory (x-axis) and activating (y-axis) ligands ranging from 0 to 100 μM , as described in Fig. 2. Four representative pVav1 response curves are shown in Fig. 2.

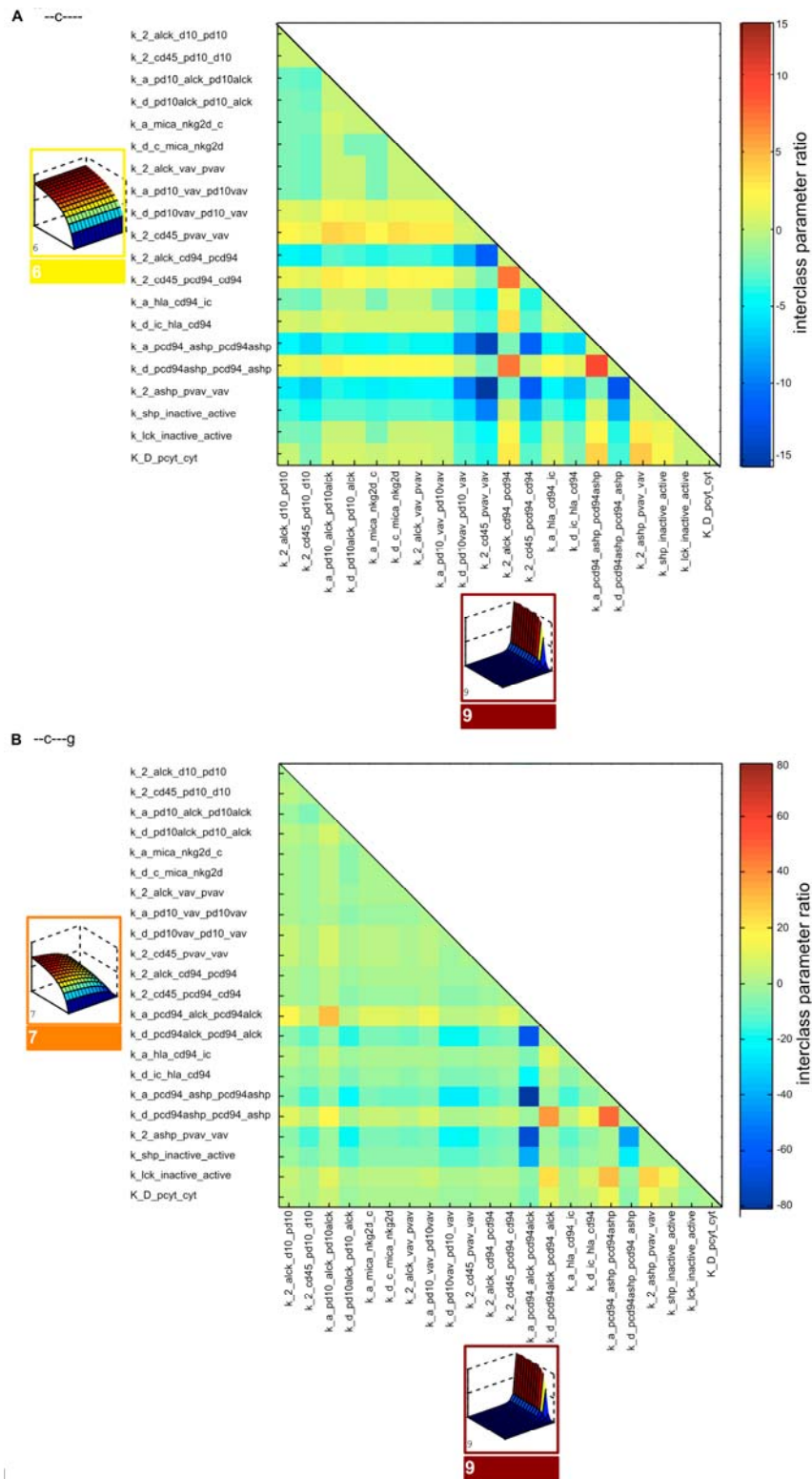


Fig. S3. Interclass parameter ratios. Parameter sets generating the different shapes were extracted from the parameter scan (Fig. 4A). For each element of the set, the parameter ratio was calculated and then geometrically averaged over the whole set. The resulting geometric mean ratio between parameters that generated a specific shape was divided by the geometric mean ratio to generate a different shape. The fold-change of this ratio is presented here. **(A)** Interclass parameter ratios of parameters that created shape 7 or shape 4 for the model “--c---” (SFk association with inhibiting and activating receptors). **(B)** Interclass parameter ratios of parameters that created shape 6 or shape 4 for the model “--c----” (SFk association with only the activating receptors). See the Supplementary Methods for more details of this approach.

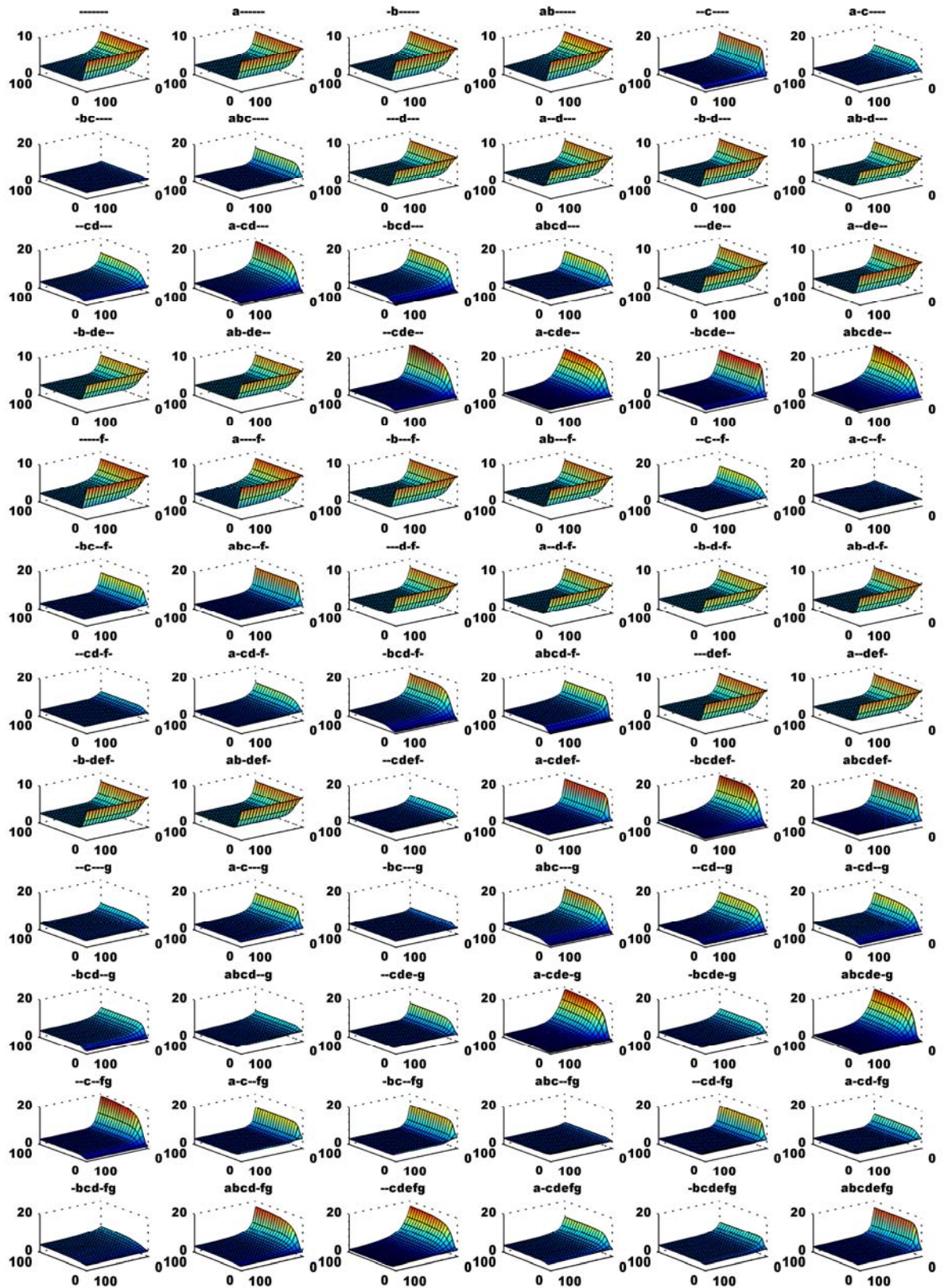


Fig. S4. Results of the parameter fit for all 72 models. Kinetic parameters of all 72 models (module codes are indicated on the top according to Fig. 1) were fitted to the experimental pVav1 dose-response behavior observed in Fig. 3. Best fitting shapes for the amount of pVav1 5 min after stimulation (z-axis, in nM) for varying amounts of inhibitory (x-axis) and activating (y axis) ligands ranging from 0 to 100 μ M are shown.

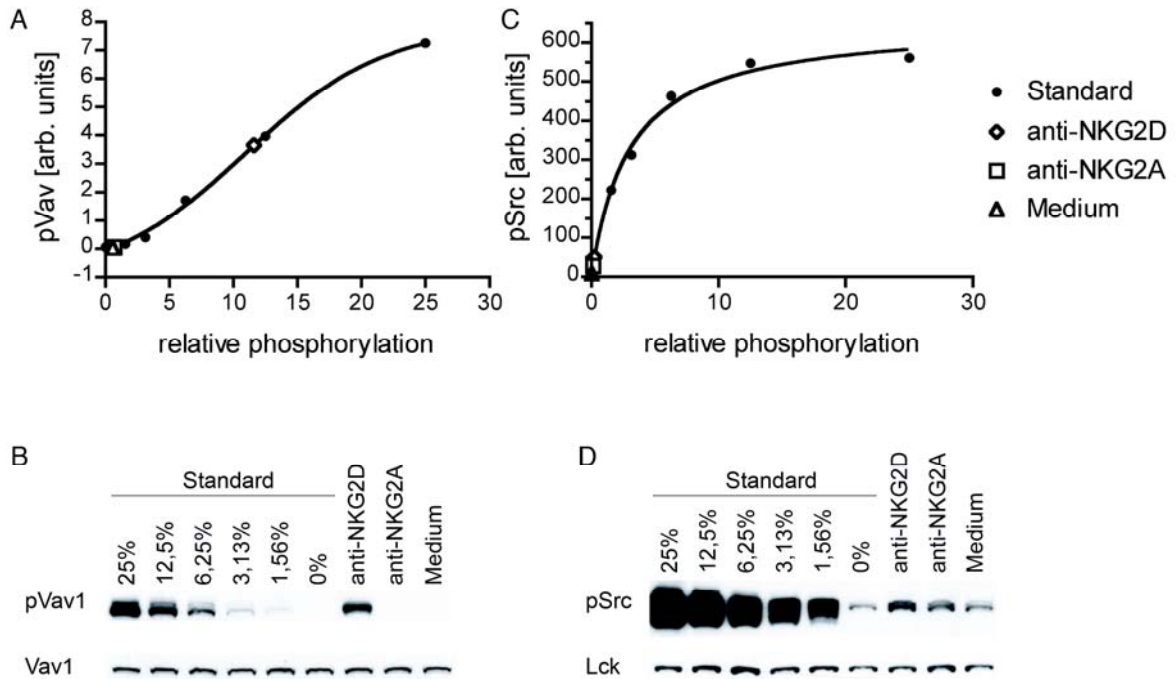


Fig. S5. Quantification of the total amounts of pVav1 and pSFK after stimulation of NK cells. The amounts of (A and B) pVav1 and (C and D) pSFK was determined by quantitative Western blotting analysis. We detected pSFK with a phosphorylation site-specific antibody (pSrc) that recognizes the phosphorylated tyrosine (pTyr⁴¹⁶) in the activation loop of SFKs and that cross-reacts with many SFKs. The intensities of the pSrc bands were normalized to those corresponding to total Lck. Through the use of cells treated with the SFK inhibitor PP1 (0% control) and the phosphatase inhibitor pervanadate (100% control) as standards (see the Supplementary Methods for details), we calculated the amounts of pVav1 and pSFK relative to those of total Vav1 and SFK. NK cells stimulated with antibody against NKG2D, antibody against NKG2A, or medium control were lysed, and the amounts of (B) pVav1 and (D) pSFK were determined by Western blotting analysis and compared to the standard curve (A, C). One experiment representative of three experiments is shown.

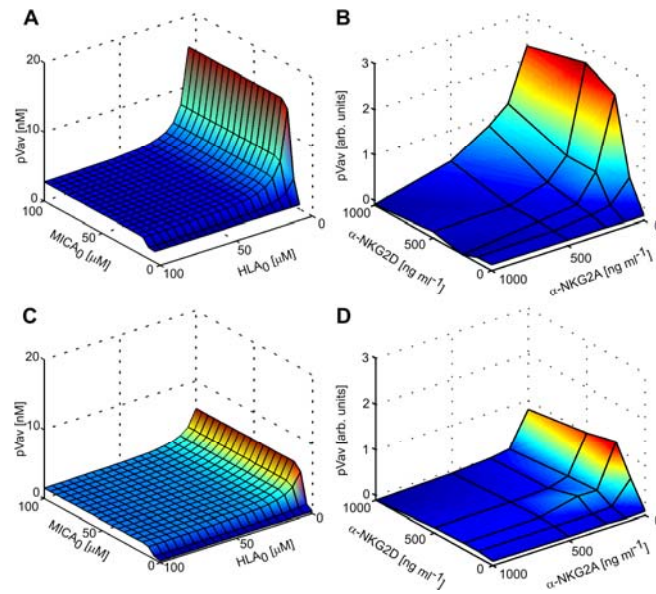


Fig. S6. Comparison between predicted and experimentally observed pVav1 responses after treatment with PP1. (A and C) Using the core model including module c and the fitted parameters described in Fig. 4, the phosphorylation of Vav1 for 5 min after target cell contact for different activating (y-axis, MICA₀) and inhibitory ligand (x-axis, HLA₀) concentrations was simulated with (A) full or (C) 50% SFK activity. The human NK cell line NKL was pretreated (D) with PP1 or (B) without PP1 for 30 min at 37°C and then incubated with the indicated concentrations of antibodies against the activating receptor NKG2D and the inhibitory receptor NKG2A. After cross-linking with secondary goat-anti-mouse antibodies, cells were incubated at 37°C for 5 min. Vav1 phosphorylation was determined as described in Fig. 3.

Table S1. Kinetic parameters used for modeling.

Reaction	Parameters	Reference	Remarks
MICA + NKG2D <-> MICA:NKG2D	$k_a = 4.3 \times 10^{-5}$ to $1.7 \times 10^{-4} \text{ nM}^{-1} \text{ s}^{-1}$ $k_d = 1.0 \times 10^{-3}$ to 0.023 s^{-1}	(2) (3)	rates are for MICA-NKG2D binding and binding of IgG to arbitrary membrane proteins, resp.
HLA E + CD94 <-> HLA E:CD94	$k_d = >1.8 \text{ s}^{-1}$	(4)	no data available for association
Y + SFK -> pY + SFK	$k_{\text{cat}} = 2.3 \times 10^{-4}$ to $98.4 \times 10^{-4} \text{ s}^{-1}$ $K_M = 2.3 \times 10^4$ to $2.17 \times 10^5 \text{ nM}$	(5)	
pY + CD45 -> Y + CD45	$k_{\text{cat}} = 1.33$ to 70 s^{-1} $K_M = 1.5 \times 10^5$ to $4 \times 10^6 \text{ nM}$	(6, 7)	
pY + SH2 <-> pY:SH2	$k_a = 1.1 \times 10^{-1} \text{ nM}^{-1} \text{ s}^{-1}$ $k_d = 0.6 \text{ s}^{-1}$	(8)	kinetic rates of the SH2-domain:phosphotyrosine binding reaction
pY + SHP-1 <-> Y + SHP1	$k_{\text{cat}} = 3$ to 200 s^{-1} $K_M = 6.6 \times 10^5$ to $2.66 \times 10^6 \text{ nM}$	(7, 9)	

Table S2. Protein numbers and concentrations for different NK cell types. Amounts of surface receptors were quantified by flow cytometry, and intracellular signaling molecules were quantified by Western blotting analysis, as described in the Supplementary Materials and in fig. S1. Numbers represent the mean value of at least three independent experiments for NKL cells and the range and mean values for flow cytometric analysis from four different donors and for Western blotting analysis from five different donors for primary human NK cells. Concentrations were calculated based on the volume of cells and the compartment the respective molecule is confined to (that is, the membrane for CD45 and the cytoplasm for Vav-1).

Protein	NKL		IL-2-expanded primary NK cells		
	Molecules per cell	Concentration (nM)	Molecules per cell range (mean)	Concentration (nM)	range
DAP10*	33,600	10,970	2,648 to 5,284 (3980)	1,402 to 2,798 (2,108)	
NKG2A	55,000	17,960	8,061 to 16,497 (12787)	4,296 to 8,737 (6,772)	
CD45	120,000	39,180	5,100 to 16,753 (11756)	2,701 to 8,873 (6,226)	
Lck	710,000	237,790	553,000 to 1,256,000 (760,000)	292,890 to 665,220 (402,520)	to
Vav1	104,000	190	79,000 to 359,000 (197,000)	920 to 4,200 (2,300)	
SHP-1	1,900,000	3,470	405,000 to 648,000 (535,000)	4,730 to 7,570 (6,250)	

*Amounts of DAP10 were taken as four times the measured numbers of NKG2D to incorporate the stoichiometry of the NKG2D-DAP10 complex and assuming that the NKG2D dimer can only bind to one antibody molecule (10).

Table S3. Table of shape functions and their analytical equations used for the classification of shapes generated in the parameter scan. After visual inspection and manual classification of 4,800 different outcomes of the parameter scan, a library of analytical equations representing the observed qualitative behaviors was compiled. To reduce the flexibility of the equations, the number of parameters in each equation was reduced to a minimum.

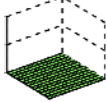
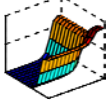
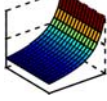
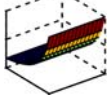
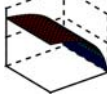
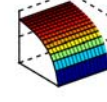
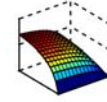
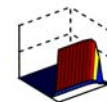
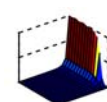
Class	Shape	Equation
1		$z = f(x, y) = \text{const.}$
2		$z = f(x, y) = 1 - \frac{1}{(1 + \frac{1}{a+x^n})} \frac{1}{(1 + \frac{1}{b+y^m})}$
3		$z = f(x, y) = \frac{1}{(a + bx)}$
4		$z = f(x, y) = \frac{1}{(a + by)}$
5		$z = f(x, y) = \frac{x}{(a + x)}$
6		$z = f(x, y) = \frac{y}{(a + y)}$
7		$z = f(x, y) = \frac{x}{(a + x)} \frac{y}{(b + y)}$
8		$z = f(x, y) = \frac{1}{(1 + y)^n} \frac{x^m}{(1 + x^m)}$
9		$z = f(x, y) = \frac{1}{(1 + x)^n} \frac{y^m}{(1 + y^m)}$

Table S4. Literature-derived and fitted kinetic rates. Each parameter is named to immediately reveal its corresponding reaction: “2”, “a”, and “d” refer to the k_{cat}/K_M values of enzymatic reactions [in $\text{nM}^{-1}\text{s}^{-1}$], the association rate [in $\text{nM}^{-1}\text{s}^{-1}$], and the dissociation rate [in s^{-1}], respectively. The following three molecule names identify: (i) the enzyme in enzymatic reactions, followed by its substrate and product; or (ii) the reactants of binding reactions, followed by the complex; or (iii) the reactant of a dissociation reaction, followed by its products. The first column represents the geometric mean values of the parameter ranges shown in table S1. An asterisk indicates a parameter that was kept constant during the parameter estimation.

Parameter	Initial value	Model			
		ab-def-	--c----	abcdef-	abcdefg
k_2_alck_d10_pd10	1.0e-08	3.4054e-07	4.5303e-07	4.5638e-07	3.9353e-08
k_2_cd45_pd10_d10	1.0e-05	1.0e-05	6.1525e-06	7.6978e-05	5.6184e-07
k_a_pd10_alck_pd10alck	1		6.773	40.448	95.251
k_d_pd10alck_pd10_alck	6		14.092	35.673	10.041
k_a_mica_nkg2d_c	8.0e-05	8.3101e-05	31.934	66.974	54.484
k_d_c_mica_nkg2d	6	6.001	19.033	97.118	19.578
k_2_palck_d10_pd10	5.0e-08	2.6037e-07		4.2305e-05	9.9833e-08
k_2_palck_alck_palck	5.0e-08	6.8906e-07		1.0429e-08	1.0974e-06
k_2_alck_alck_palck	1.0e-08	1.1055e-08		6.6976e-09	2.887e-07
k_2_cd45_palck_alck	1.0e-05	8.0168e-06		1.6915e-05	1.7271e-06
k_2_alck_vav_pvav	1.0e-08	7.1675e-07	1.4271e-06	1.0938e-06	4.2025e-07
k_2_palck_vav_pvav	5.0e-08	5.0794e-08		1.3108e-07	1.7451e-06
k_a_pd10_vav_pd10vav	1	10.005	90.315	11.858	26.588
k_d_pd10vav_pd10_vav	6	60.049	60.155	3.057	54.327
k_2_cd45_pvav_vav	1.0e-05	1.0e-05	1.245e-07	3.0333e-06	2.3575e-07
k_2_alck_cd94_pcd94	1.0e-08	1.6138e-07	1.3217e-07	4.3432e-07	1.1508e-09
k_2_cd45_pcd94_cd94	1.0e-05	6.217e-06	4.5829e-05	3.8518e-06	2.517e-05
k_a_pcd94_alck_pcd94alck	1				1.289
k_d_pcd94alck_pcd94_alck	6				87.197
k_a_hla_cd94_ic	8.0e-05	7.98e-05	6.0876e-06	14.302	4.2257e-05
k_d_ic_hla_cd94	6	60.021	39.547	71.985	54.055
k_2_palck_cd94_pcd94	5.0e-08	5.0479e-08		4.5981e-08	3.1925e-08
k_2_alck_ashp_pashp	1.0e-08	1.1365e-08		1.755e-06	2.6017e-10
k_2_palck_ashp_pashp	5.0e-08	5.5077e-		1.3577e-	8.9795e-

		08		05	12
k_a_pcd94_ashp_pcd94ashp	1	10.002	76.864	173	12.243
k_d_pcd94ashp_pcd94_ashp	6	60.016	20.783	74.784	29.069
k_2_cd45_pashp_ashp	1.0e-05	1.3319e-05		1.9144e-06	8.559e-05
k_2_pashp_pvav_vav	5.0e-05	4.9971e-05		52.984	61.915
k_2_pashp_palck_alck	5.0e-05	4.9963e-05		1.5542e-05	3.2563e-06
k_c_cd45is_cd45	2.0e-05	1.9982e-05		3.9757e-05	6.6754e-06
k_2_pvav_pd10_pd10is	2.0e-05	2.0581e-05		5.995	3.3774e-07
k_2_ashp_palck_alck	1.0e-05	9.9712e-06		4.8696e-07	2.5772e-07
k_2_ashp_pvav_vav	1.0e-05	1.1283e-05	2.051e-05	9.0644e-05	1.212
k_shp_inactive_active	1	10.033	30.409	1.683	89.396
k_lck_inactive_active	1	10.013	53.428	14.871	55.115
k_shp_active_inactive*	1	1	1	1	1
k_lck_active_inactive*	1	1	1	1	1
K_D_pcyt_cyt	5	50.029	11.211	11.283	85.207

References

1. B. B. Aldridge, J. M. Burke, D. A. Lauffenburger, P. K. Sorger, Physicochemical modelling of cell signalling pathways. *Nat. Cell. Biol.* **8**, 1195–1203 (2006).
2. B. J. McFarland, R. K. Strong, Thermodynamic analysis of degenerate recognition by the NKG2D immunoreceptor: not induced fit but rigid adaptation. *Immunity* **19**, 803–812 (2003).
3. H. Mitomo, H. Shigematsu, E. Kobatake, H. Furusawa, Y. Okahata, IgG binding kinetics to oligo B protein A domains on lipid layers immobilized on a 27 MHz quartz-crystal microbalance. *J. Mol. Recognit.* **20**, 83–89 (2007).
4. M. Vales-Gomez, H. T. Reyburn, R. A. Erskine, M. Lopez-Botet, J. L. Strominger, Kinetics and peptide dependency of the binding of the inhibitory NK receptor CD94/NKG2-A and the activating receptor CD94/NKG2-C to HLA-E. *EMBO J.* **18**, 4250–4260 (1999).
5. H. R. Housden, P. J. Skipp, M. P. Crump, R. J. Broadbridge, T. Crabbe, M. J. Perry, M. G. Gore, Investigation of the kinetics and order of tyrosine phosphorylation in the T-cell receptor zeta chain by the protein tyrosine kinase Lck. *Eur. J. Biochem.* **270**, 2369–2376 (2003).
6. J. Felberg, P. Johnson, Characterization of recombinant CD45 cytoplasmic domain proteins. Evidence for intramolecular and intermolecular interactions. *J. Biol. Chem.* **273**, 17839–17845 (1998).
7. G. H. Peters, S. Branner, K. B. Moller, J. N. Andersen, N. P. Moller, Enzyme kinetic characterization of protein tyrosine phosphatases. *Biochimie* **85**, 527–534 (2003).
8. N. J. de Mol, E. Plomp, M. J. Fischer, R. Ruijtenbeek, Kinetic analysis of the mass transport limited interaction between the tyrosine kinase lck SH2 domain and a phosphorylated peptide studied by a new cuvette-based surface plasmon resonance instrument. *Anal. Biochem.* **279**, 61–70 (2000).
9. T. Niu, X. Liang, J. Yang, Z. Zhao, G. W. Zhou, Kinetic comparison of the catalytic domains of SHP-1 and SHP-2. *J. Cell. Biochem.* **72**, 145–150 (1999).
10. D. Garrity, M. E. Call, J. Feng, K. W. Wucherpfennig, The activating NKG2D receptor assembles in the membrane with two signaling dimers into a hexameric structure. *Proc. Natl. Acad. Sci. U.S.A.* **102**, 7641–7646 (2005).